



Self-assembly and structures of new transition metal complexes with phenyl substituted pyrazole carboxylic acid and N-donor co-ligands

Chong-Bo Liu^{a,*}, Yun-Nan Gong^a, Yuan Chen^a, Hui-Liang Wen^b

^a School of Environment and Chemical Engineering, Nanchang Hangkong University, Nanchang, Jiangxi 330063, China

^b State Key Laboratory of Food Science and Technology, Nanchang University, Nanchang, Jiangxi 330047, China

ARTICLE INFO

Article history:

Received 18 July 2011

Received in revised form 11 October 2011

Accepted 8 November 2011

Available online 27 November 2011

Keywords:

Pyrazole carboxylic acid

N-donor co-ligands

Transition metal complexes

Channels

Homohelical chain

Properties

ABSTRACT

Five new transition metal complexes, $[\text{Ni}(\text{HL}^1)_2(2,2'\text{-bipy})]\cdot 3\text{H}_2\text{O}$ (**1**), $[\text{Ni}(\text{HL}^1)_2(4,4'\text{-bipy})]$ (**2**), $[\text{Co}(\text{HL}^1)_2(4,4'\text{-bipy})]\cdot 5\text{H}_2\text{O}$ (**3**), $[\text{Ni}_2(\text{HL}^2)_4(4,4'\text{-bipy})\cdot (\text{H}_2\text{O})_2]\cdot 4\text{H}_2\text{O}$ (**4**), $[\text{Co}(\text{HL}^2)_2(4,4'\text{-bipy})]$ (**5**) ($\text{H}_2\text{L}^1 = 5\text{-phenyl-1H-pyrazole-3-carboxylic acid}$; $\text{H}_2\text{L}^2 = 3\text{-phenyl-1H-pyrazole-4-carboxylic acid}$; $2,2'\text{-bipy} = 2,2'\text{-bipyridine}$; $4,4'\text{-bipy} = 4,4'\text{-bipyridine}$) have been synthesized and characterized. Complex **1** exhibits a monomeric structure, **2** and **3** display 1D chain structures, **4** and **5** possess 3D metal-organic frameworks with 1D channels, and all extend to 3D supramolecular networks via rich hydrogen bonds. Complex **4** shows a new (4,6)-connected network with $(4^4.5^8.6^3)(5^4.6-8)$ topology, while **5** exhibits a NaCl-like network with $(4^{12}.6^3)$ topology. The thermal stabilities of complexes **1–5** and powder XRD of **4** and **5** were investigated. Furthermore, the antibacterial activities of the title complexes against the tested bacteria were studied and compared to the activities of the corresponding free ligands.

© 2011 Elsevier B.V. All rights reserved.

1. Introduction

In recent years, considerable research efforts have been directed towards the design and synthesis of metal-organic complexes not only because of their fascinating structural diversities, but also due to their potential applications in ion exchange, biological activities, magnetic and porous materials [1–7]. In general, the structures of the complexes depend on the combination of several factors, including metal ions, organic ligands, pH value, reaction temperature, etc. [8–11]. So, proper selection of metal ions and organic ligands is a key issue in designing and self-assembly of new metal-organic complexes.

Especially, multidentate carboxylate ligands with N- and O-donors have received much more attention due to their high access to metals, to form 3d, 4f or 3d–4f metal-organic complexes, and pyrazole carboxylic acid compound is a good example of N- and O-donors ligands and regarded as one kind of elegant ligands [12–17]. Whereas, very few complexes of pyrazole carboxylic acids except 3,5-pyrazoledicarboxylic acid have been reported [18–24]. One phenyl group is introduced to pyrazole carboxylic acid, which increases the possibility of π - π and C-H \cdots π interactions, and help to construct high-dimensional supramolecular structures [25,26]. In this paper, we synthesized two kinds of phenyl substituted pyrazole carboxylic acid: 5-phenyl-1H-pyrazole-3-carboxylic acid (H_2L^1) and

3-phenyl-1H-pyrazole-4-carboxylic acid (H_2L^2) [27–30], to investigate the influence of different positions of carboxylate groups on the structures. On the other hand, metal ions due to their different radii and coordination geometry, and auxiliary ligands due to their different sizes and coordination modes, often have significant effect on the formation and the structures of complexes [31–33]. In particular, 4,4'-bipy as linear bridging auxiliary ligand is often used to construct high-dimensional porous metal-organic frameworks [34,35]. Herein we report the syntheses and the structures of five new transition metal complexes with H_2L^1 and H_2L^2 , and N-donor co-ligands: $[\text{Ni}(\text{HL}^1)_2(2,2'\text{-bipy})]\cdot 3\text{H}_2\text{O}$ (**1**), $[\text{Ni}(\text{HL}^1)_2(4,4'\text{-bipy})]$ (**2**), $[\text{Co}(\text{HL}^1)_2(4,4'\text{-bipy})]\cdot 5\text{H}_2\text{O}$ (**3**), $[\text{Ni}_2(\text{HL}^2)_4(4,4'\text{-bipy})\cdot (\text{H}_2\text{O})_2]\cdot 4\text{H}_2\text{O}$ (**4**), $[\text{Co}(\text{HL}^2)_2(4,4'\text{-bipy})]$ (**5**).

2. Experimental

2.1. Materials and measurements

5-Phenyl-1H-pyrazole-3-carboxylic acid (H_2L^1) and 3-phenyl-1H-pyrazole-4-carboxylic acid (H_2L^2) were prepared according to literature method [27–30]. All other reagents were commercially available and used without further purification. Elemental analysis of C, H and N were carried out with an Elementar Vario EL analyzer. Infrared spectra were recorded with a Nicolet Avatar 360 FT-IR spectrometer using the KBr pellet technique. ¹H NMR spectra were recorded at 400 MHz on a Bruker WH400 DS spectrometer. Thermal stability studies were carried out on a ZRY-2P Thermal Analyzer.

* Corresponding author. Tel./fax: +86 791 6453231.

E-mail address: cblu@nchu.edu.cn (C.-B. Liu).

X-ray powder diffraction patterns were recorded on D8 ADVANCE X-ray diffractometer.

2.2. Synthesis of $[Ni(HL^1)_2(2,2'-bipy)] \cdot 3H_2O$ (**1**)

A mixture of $NiCl_2 \cdot 6H_2O$ (0.024 g, 0.1 mmol), H_2L^1 (0.019 g, 0.1 mmol), 2,2'-bipyridine (0.016 g, 0.1 mmol), NaOH (0.15 mL, 0.65 M) and distilled water (10 mL) was sealed in a Teflon-lined stainless reactor (23 mL) and heated 120 °C for 72 h under autogenous pressure. Blue block crystals were obtained. Yield: 43.5%. *Anal. Calc.* for $C_{30}H_{28}NiN_6O_7$: C, 56.01; H, 4.35; N, 13.07. Found: C, 56.46; H, 4.18; N, 13.55%. IR data (KBr pellet, ν/cm^{-1}): 3409 s, 1602 s, 1495 m, 1413 s, 1337 s, 1207 w, 1023 m, 957 w, 918 w, 829 m, 761 m.

2.3. Synthesis of $[Ni(HL^1)_2(4,4'-bipy)]$ (**2**)

The synthesis of **2** was similar with that of **1**, only that 0.1 mmol 4,4'-bipyridine was used instead of 0.1 mmol 2,2'-bipyridine, NaOH aqueous solution was reduced to 0.1 mL and the temperature of the reaction mixture was 150 °C. Blue block crystals were obtained. Yield: 54.5%. *Anal. Calc.* for $C_{30}H_{22}NiN_6O_4$: C, 61.15; H, 3.76; N, 14.27. Found: C, 61.33; H, 3.55; N, 14.55%. IR data (KBr pellet, ν/cm^{-1}): 1634 s, 1583 s, 1488 m, 1414 s, 1339 s, 1297 s, 1209 m, 1097 m, 942 w, 807 m, 663 w.

2.4. Synthesis of $[Co(HL^1)_2(4,4'-bipy)] \cdot 5H_2O$ (**3**)

The synthesis of **3** was similar with that of **2**, only that 0.1 mmol $CoCl_2 \cdot 6H_2O$ was used instead of 0.1 mmol $NiCl_2 \cdot 6H_2O$ and the temperature of the reaction mixture was 90 °C. Red block crystals were obtained. Yield: 42.3%. *Anal. Calc.* for $C_{30}H_{32}CoN_6O_9$: C, 53.02; H, 4.75; N, 12.37. Found: C, 53.25; H, 4.52; N, 12.65%. IR data (KBr pellet, ν/cm^{-1}): 3134 m, 1608 s, 1495 m, 1413 s, 1337 m, 1208 m, 1073 m, 974 w, 889 w, 824 m, 761 m, 685 m.

2.5. Synthesis of $[Ni_2(HL^2)_4(4,4'-bipy) \cdot (H_2O)_2] \cdot 4H_2O$ (**4**)

A mixture of $NiCl_2 \cdot 6H_2O$ (0.024 g, 0.1 mmol), H_2L^2 (0.019 g, 0.1 mmol), 4,4'-bipyridine (0.016 g, 0.1 mmol), NaOH (0.15 mL, 0.65 M) and distilled water (10 mL) was sealed in a Teflon-lined stainless reactor (23 mL) and heated 120 °C for 72 h under autogenous

pressure. Green block crystals were obtained. Yield: 36.5%. *Anal. Calc.* for $C_{50}H_{48}Ni_{10}Ni_2O_{14}$: C, 53.12; H, 4.37; N, 12.39. Found: C, 53.49; H, 4.12; N, 12.55%. IR data (KBr pellet, ν/cm^{-1}): 3147 m, 1607 m, 1537 m, 1490 m, 1402 m, 1327 s, 1220 w, 959 m, 915 w, 810 m, 758 w, 693 m.

2.6. Synthesis of $[Co(HL^2)_2(4,4'-bipy)]$ (**5**)

The synthesis of **5** was similar with that of **4**, only that 0.1 mmol $CoCl_2 \cdot 6H_2O$ was used instead of 0.1 mmol $NiCl_2 \cdot 6H_2O$. Red block crystals were obtained. Yield: 58.5%. *Anal. Calc.* for $C_{30}H_{22}Ni_6CoO_4$: C, 61.12; H, 3.76; N, 14.26. Found: C, 61.45; H, 3.52; N, 14.03%. IR data (KBr pellet, ν/cm^{-1}): 1615 m, 1545 s, 1488 m, 1433 m, 1334 s, 1275 w, 1083 m, 957 s, 899 m, 805 m, 768 w, 701 w.

2.7. X-ray crystallographic study

The X-ray single-crystal data of complexes **1–5** were recorded on a Bruker APEX II area detector diffractometer with a graphite-monochromated Mo K α radiation ($\lambda = 0.71073 \text{ \AA}$). Semi-empirical absorption corrections were applied to the title complexes using the SADABS program [36]. The structures were solved by direct methods [37] and refined by full-matrix least squares on F^2 using SHELXL-97 [38]. All non-hydrogen atoms were refined anisotropically. Hydrogen atoms were placed in geometrically calculated positions. Experimental details for X-ray data collection of **1–5** are presented in Table 1, selected bond lengths are listed in Table 2, and the types of hydrogen bonds are listed in Table 3.

2.8. Antibacterial testing

The *in vitro* antibacterial activities of H_2L^1 and H_2L^2 , and complexes **1–5** were tested against Gram positive bacteria: *Staphylococcus aureus*, *Canidia albicans* and *Bacillus subtilis*, and Gram negative bacteria: *Escherichia coli* and *Pseudomonas aeruginosa* by minimum inhibitory concentration (MIC) method. The compounds were dissolved in DMF with twofold serial dilutions from 200 to 6.25 $\mu\text{g/mL}$. Sterile micro tubes were filled with 1 mL of serial twofold dilutions of compounds. A growth tube (broth plus inoculum) and a sterility control tube (broth only) were included in each time. The tubes were incubated at 37 °C for 24 h. MICs were defined as

Table 1
Crystal data for complexes **1–5**.

Complex	1	2	3	4	5
Empirical formula	$C_{30}H_{28}NiN_6O_7$	$C_{30}H_{22}NiN_6O_4$	$C_{30}H_{32}CoN_6O_9$	$C_{50}H_{48}Ni_{10}Ni_2O_{14}$	$C_{30}H_{22}CoN_6O_4$
Formula weight	643.29	589.25	679.55	1130.41	589.47
T (K)	296(2)	296(2)	296(2)	296(2)	296(2)
Crystal system	rhombohedral	monoclinic	tetragonal	monoclinic	monoclinic
Space group	$R\bar{3}c$	Cc	$P4_322$	$I2/a$	$C2/c$
a (\AA)	27.013(8)	14.483(4)	11.4214(5)	12.6652(9)	24.038(3)
b (\AA)	27.013(8)	17.050(5)	11.4214(5)	11.4083(8)	12.7537(16)
c (\AA)	21.432(7)	13.026(4)	24.2401(11)	34.571(3)	11.8640(15)
α ($^\circ$)	90	90	90	90	90
β ($^\circ$)	90	121.296(3)	90	97.5210(10)	110.073(2)
γ ($^\circ$)	120	90	90	90	90
V (\AA^3)	13544(7)	2748.7(14)	3162.1(2)	4952.2(6)	3416.3(7)
Z	18	4	4	4	4
F(000)	6012	1216	1412	2344	1212
D_{calc} (mg m^{-3})	1.420	1.424	1.427	1.516	1.146
θ range ($^\circ$)	2.49–25.50	2.39–27.50	2.45–25.50	2.41–27.50	2.36–25.50
μ (mm^{-1})	0.701	0.753	0.605	0.840	0.541
GOF	2.373	1.392	1.036	1.014	1.078
Reflections/collected	34149/2813	11751/5819	24585/2953	21392/5657	13039/3186
Unique (R_{int})	0.0568	0.0404	0.0363	0.0319	0.0498
R_1, wR_2 [$I > 2\sigma(I)$]	0.0399, 0.0476	0.0460, 0.0942	0.0433, 0.1141	0.0420, 0.0897	0.0452, 0.1296
R_1, wR_2 (all data)	0.0617, 0.0491	0.0503, 0.0957	0.0510, 0.1214	0.0594, 0.1005	0.0547, 0.1354

Table 2
Selected bond lengths (Å) for complexes 1–5.

1			
Ni(1)–O(1)	2.0656(14)	Ni(1)–O(1) ^{#1}	2.0657(14)
Ni(1)–N(1)	2.0867(17)	Ni(1)–N(1) ^{#1}	2.0867(17)
Ni(1)–N(3)	2.0595(18)	Ni(1)–N(3) ^{#1}	2.0594(18)
Symmetry operation: #1 $x + 2/3, y - 2/3, -z + 13/6$			
2			
Ni(1)–O(2)	2.058(2)	Ni(1)–O(3)	2.109(2)
Ni(1)–N(2)	2.095(3)	Ni(1)–N(4)	2.114(3)
Ni(1)–N(5)	2.050(3)	Ni(1)–N(6) ^{#1}	2.069(3)
Symmetry operation: #1 $x + 1/2, y + 1/2, z$			
3			
Co(1)–O(1)	2.059(3)	Co(1)–O(1) ^{#1}	2.059(3)
Co(1)–N(1)	2.113(3)	Co(1)–N(1) ^{#1}	2.113(3)
Co(1)–N(3)	2.178(4)	Co(1)–N(4) ^{#2}	2.161(3)
Symmetry operations: #1 $-x + 1, y, -z$; #2 $x, y + 1, z$			
4			
Ni(1)–O(1)	2.0392(18)	Ni(1)–O(1) ^{#1}	2.0391(18)
Ni(1)–O(5)	2.102(2)	Ni(1)–O(5) ^{#1}	2.102(2)
Ni(1)–N(3)	2.133(3)	Ni(1)–N(4) ^{#2}	2.159(3)
Ni(2)–O(4) ^{#3}	2.0944(18)	Ni(2)–O(4) ^{#4}	2.0943(18)
Ni(2)–N(1)	2.123(2)	Ni(2)–N(1) ^{#5}	2.123(2)
Ni(2)–N(6)	2.067(2)	Ni(2)–N(6) ^{#5}	2.067(2)
Symmetry operations: #1 $-x + 1/2, y, -z + 1$; #2 $x, y + 1, z$; #3 $x + 1/2, -y + 1, z$; #4 $-x, y - 1/2, -z + 1/2$; #5 $-x + 1/2, -y + 1/2, -z + 1/2$			
5			
Co(1)–O(1) ^{#1}	2.1444(15)	Co(1)–O(1) ^{#2}	2.1444(15)
Co(1)–N(1)	2.111(2)	Co(1)–N(1) ^{#3}	2.111(2)
Co(1)–N(3)	2.195(2)	Co(1)–N(3) ^{#3}	2.195(2)
Symmetry operations: #1 $-x + 1/2, y + 1/2, -z + 3/2$; #2 $x, -y, z + 1/2$; #3 $-x + 1/2, -y + 1/2, -z + 2$			

the lowest concentrations of compounds which inhibit the growth of microorganisms, DMF was inactive under applied conditions.

3. Results and discussion

3.1. Crystal structure of $[Ni(HL^1)_2(2,2'-bipy)] \cdot 3H_2O$ (**1**)

Single crystal X-ray diffraction analysis reveals that the asymmetric unit of complex **1** contains one Ni(II) ion, two HL¹ ligands, one 2,2'-bipy and three lattice water molecules. Each Ni(II) ion in complex **1** lies on an inversion center and coordinates to six atoms: two carboxylate oxygen atoms and two nitrogen atoms from two HL¹ ligands, another two nitrogen atoms from one 2,2'-bipy molecule, as shown in Fig. 1. In **1**, HL¹ and 2,2'-bipy ligands adopt N,O-chelating and N,N-chelating modes to coordinate to Ni(II) ion (as shown in Scheme 1a), respectively, and the phenyl and pyrazole rings of HL¹ ligands are twisted by an angle of 5.1°. In **1**, there exist abundant hydrogen bonds: (a) between lattice water molecules and carboxylate oxygen atoms; (b) between N–H of pyrazole rings and lattice water molecules; (c) between C–H of phenyl or pyridine rings and lattice water molecules (Table 3). Each monomeric entity of complex **1** is linked with neighbors via O–H...O hydrogen bonds to give rise to 1D zig-zag chain along the *c* axis (Fig. 2a), which extend to a 3D supramolecular network via N–H...O and C–H...O hydrogen bonds (Fig. 2b).

3.2. Crystal structure of $[Ni(HL^1)_2(4,4'-bipy)]$ (**2**)

As shown in Fig. 3, each Ni(II) ion in complex **2** coordinates to six atoms: four nitrogen atoms from two HL¹ ligands and two 4,4'-bipy molecules, leaving two *cis*-positions for two carboxylate oxygen atoms of two HL¹ ligands. Similar to **1**, HL¹ ligands also adopt N,O-chelating mode coordinating to Ni(II) ion in **2**. However, there are two orientations of HL¹ ligands in **2** with the dihedral angles between phenyl and pyrazole rings of 9.3° and 22.3°,

respectively. Furthermore, 4,4'-bipy molecules act as bridging ligand linking the Ni(II) ions into 1D chain (Fig. 4a). In **2**, there are rich N–H...O hydrogen bonds between N–H of pyrazole rings and carboxylate oxygen atoms, and C–H...O hydrogen bonds between

C–H of pyridine rings and carboxylate oxygen atoms (Table 3), which extend 1D chains into a 3D supramolecular network with rhombus channels (ca. 11.19 × 11.19 Å²) along the *c* axis (Fig. 4b).

3.3. Crystal structure of $[Co(HL^1)_2(4,4'-bipy)] \cdot 5H_2O$ (**3**)

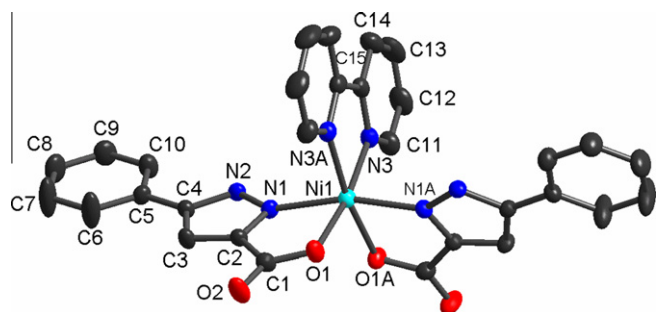
Complex **3** crystallize in chiral space group *P*₄322, as a new example of homochiral crystallization of helical coordination polymers. In complex **3**, Co(II) ion is coordinated by four nitrogen atoms from two HL¹ ligands and two 4,4'-bipy molecules, different from **2**, leaving two *trans*-positions for two carboxylate oxygen atoms of two HL¹ ligands (Fig. 5). In **3** HL¹ ligands only have one orientation, and the phenyl and pyrazole rings are almost coplanar with the dihedral angle of 1.9°. In **3**, each HL¹ ligand chelates one Co(II) ion, and each 4,4'-bipy molecule bridges two Co(II) ions, which lead to 1D chains, furthermore, O–H...O hydrogen bonds between carboxylate oxygen atoms and lattice water molecules and N–H...O hydrogen bonds between N–H of pyrazole rings and lattice water molecules join the chains to a 3D supramolecular network, as shown in Fig. 6a. An interesting feature of complex **3** is its double-stranded homohelical chain structure, the repeating unit of which can be described as $-(O4...HL^1)_{-4n}$, and the pitch of the helix running along the *c*-axis is the same as its length (24.24 Å), two antiparallel helical chains with the same chirality intertwine to form a left-handed double helix, as shown in Fig. 6b.

3.4. Crystal structure of $[Ni_2(HL^2)_4(4,4'-bipy) \cdot (H_2O)_2] \cdot 4H_2O$ (**4**)

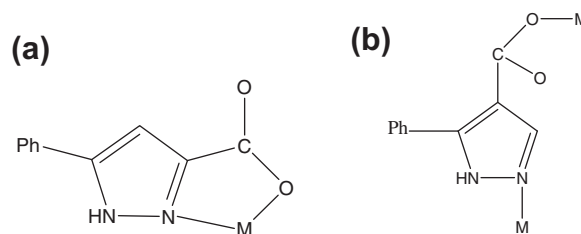
Single crystal X-ray diffraction shows that complex **4** contains two crystallographically independent Ni(II) centers. As shown in Fig. 7, Ni1 is not located at a symmetry center and coordinates to

Table 3
Hydrogen bonding geometry (Å and °) for complexes 1–5.

D–H...A	d(D–H)	d(H...A)	d(D...A)	∠DHA
1				
O(3)–H(1W)···O(2) ^{#1}	0.84	1.95	2.779(2)	172.9
O(3)–H(2W)···O(2) ^{#2}	0.84	1.95	2.756(2)	160.8
O(4)–H(3W)···O(1) ^{#3}	0.83	1.96	2.771(18)	166.7
N(2)–H(2)···O(3) ^{#4}	0.87	1.89	2.751(2)	173.3
C(10)–H(10)···O(3) ^{#4}	0.93	2.34	3.243(4)	165.0
C(14)–H(14)···O(4) ^{#5}	0.93	2.35	3.282(3)	178.0
C(14)–H(14)···O(4) ^{#6}	0.93	2.35	3.282(3)	178.0
Symmetry operations: #1 $-x + 2/3, -y + 4/3, -z + 4/3$; #2 $x + 1, y, z - 1$; #3 $x, y, z - 1$; #4 $-x + y + 1/3, -x + 5/3, z + 2/3$; #5 $-x + y + 1/3, y - 1/3, -z + 4/3$; #6 $-x + y + 1/3, y + 1/3, z + 5/6$				
2				
N(1)–H(1)···O(4) ^{#1}	0.86	2.02	2.854(4)	163.6
N(3)–H(3A)···O(4) ^{#1}	0.86	1.94	2.755(5)	156.9
C(24)–H(24)···O(2) ^{#1}	0.93	2.54	3.461(5)	173.0
C(25)–H(25)···O(3) ^{#1}	0.93	2.47	3.271(4)	144.0
C(29)–H(29)···O(2) ^{#1}	0.93	2.54	3.434(4)	162.0
C(30)–H(30)···O(1) ^{#1}	0.93	2.47	3.047(5)	120.0
Symmetry operation: #1 $x, -y, z + 1/2$				
3				
O(3)–H(1W)···O(1) ^{#1}	0.84	2.16	2.902(7)	147.7
O(3)–H(2W)···O(4) ^{#2}	0.83	1.56	2.379(13)	164.6
O(4)–H(3W)···O(5) ^{#3}	0.87	2.57	3.235(17)	133.7
O(4)–H(4W)···O(2) ^{#1}	0.90	2.39	3.000(8)	124.7
O(4)–H(4W)···O(2) ^{#4}	0.90	2.46	3.223(11)	142.4
O(5)–H(5W)···O(2) ^{#5}	0.80	2.54	3.050(10)	123.1
N(2)–H(3)···O(3) ^{#3}	0.86	1.93	2.677(7)	145.1
N(2)–H(3)···O(4) ^{#6}	0.86	2.52	3.226(10)	140.3
Symmetry operations: #1 $x, y, z + 1$; #2 $-x + 1, -y + 1, -z + 7/4$; #3 $-x + 1, y, -z + 1$; #4 $-x, y, -z + 1$; #5 $-x + 1, y, z + 1/4$; #6 $-x + 1, y, z - 3/4$				
4				
O(5)–H(1W)···O(6)	0.83	1.96	2.772(3)	166.5
O(5)–H(2W)···O(2)	0.83	1.93	2.721(3)	160.6
O(6)–H(3W)···O(7) ^{#1}	0.83	2.32	2.855(4)	123.1
O(7)–H(6W)···O(2)	0.84	2.04	2.770(4)	145.3
O(7)–H(5W)···O(3) ^{#2}	0.84	2.30	2.887(3)	127.8
N(2)–H(2A)···O(4) ^{#3}	0.86	2.21	2.746(3)	120.0
N(5)–H(5A)···O(3) ^{#3}	0.86	1.96	2.728(3)	148.1
Symmetry operations: #1 $-x + 1, -y + 1, -z + 1$; #2 $x + 1/2, -y + 1, z$; #3 $-x, y - 1/2, -z + 1/2$				
5				
N(2)–H(2D)···O(2) ^{#1}	0.86	1.91	2.679(3)	148.8
C(11)–H(11)···O(1) ^{#2}	0.93	2.41	2.981(4)	120.0
Symmetry operations: #1 $-x + 1/2, y + 1/2, -z + 3/2$; #2 $x, -y, z + 1/2$				

**Fig. 1.** The coordination environment of Ni(II) ion in complex 1 with 30% thermal ellipsoids. All hydrogen atoms are omitted for clarity (symmetry operation: A: $x + 2/3, y - 2/3, -z + 13/6$).

six atoms: four oxygen atoms from two HL² ligands and two water molecules, and two nitrogen atoms from two 4,4'-bipy molecules. However, Ni²⁺ is located at a symmetry center and surrounded by two oxygen atoms and four nitrogen atoms from six HL² ligands. In 4, HL² ligands adopt bis(monodentate) bridging mode (as shown in Scheme 1b), and have two orientations with the dihedral angles

**Scheme 1.** The coordination modes of H₂L¹ (a) and H₂L² (b) ligands in the title complexes.

between phenyl and pyrazole rings of 11.4° and 49.3°, respectively. HL² and 4,4'-bipy ligands link the Ni(II) ions into a 3D metal-organic framework with 1D channels (ca. 6.17 × 8.27 Å²) along the a axis (Fig. 8a). Moreover, the lattice water molecules are trapped in the channels through O–H...O hydrogen bonds between carboxylate oxygen atoms and water molecules (Table 3).

In 4, a better insight into the 3D framework can be achieved by application of a topological approach, each Ni1 links two HL² ligands and two 4,4'-bipy molecules, which can be viewed as a four-connected node, and each Ni2 links six HL² ligands, which

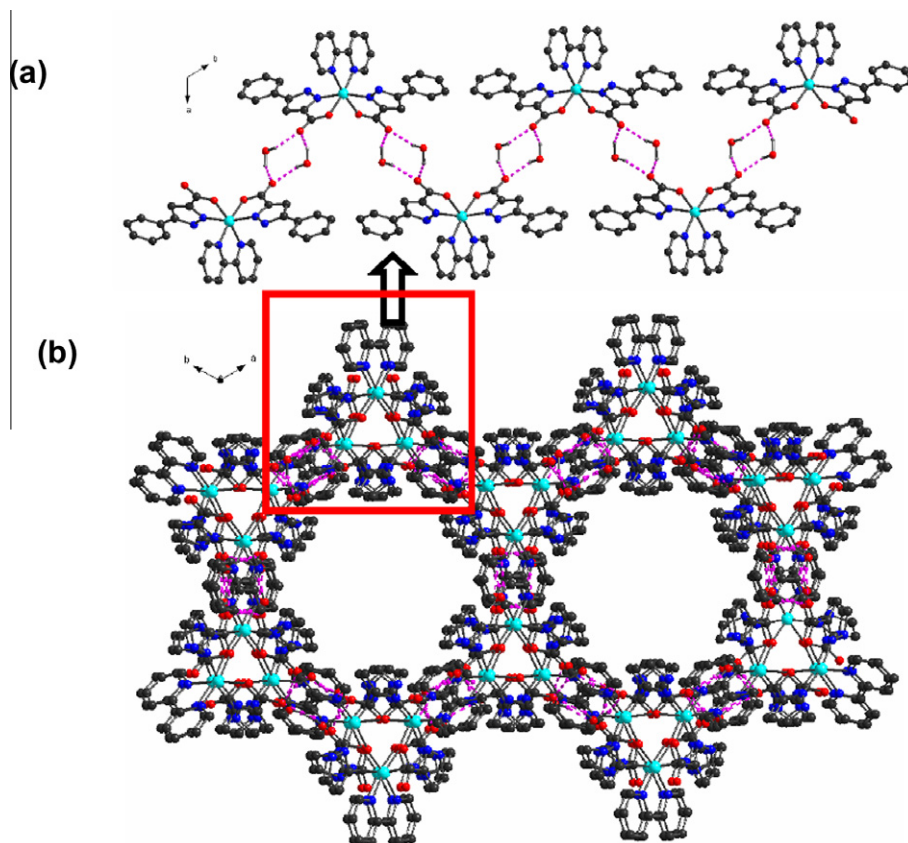


Fig. 2. (a) View of 1D zig-zag chain of complex **1** along the *c* axis; (b) The 3D supramolecular network of **1** along the *c* axis, the phenyl rings of HL¹ ligands are omitted for clarity.

3.5. Crystal structure of [Co(HL²)₂-(4,4'-bipy)] (**5**)

The Co(II) ion in complex **5** lies on an inversion center, displaying a distorted octahedral geometry, coordinating to two carboxylate oxygen and two nitrogen atoms from two HL² ligands, another two nitrogen atoms from two 4,4'-bipy molecules, as shown in Fig. 9. In **5**, HL² ligands adopt the same coordination mode as it in **4**, while there is only one orientation of HL² ligand with the dihedral angle between phenyl and pyrazole rings of 52.4°. In **5**, HL² ligands link the Co(II) ions into a 2D layer structure, and 4,4'-bipy molecules further link these 2D layers to a 3D metal–organic framework with 1D channels along the *b* axis, the size of the channel is about 11.43 × 8.71 Å² based on the distance between adjacent Co atoms (Fig. 10a).

Topologically, each Co(II) ion links four HL² ligands and two 4,4'-bipy molecules, which can be viewed as a six-connected node, so the overall structure can be simplified to a six-connected NaCl-like network with (4¹²·6³) topology (Fig. 10b).

3.6. Effect of the reaction system on structural diversity

3.6.1. The position of carboxylate group on the pyrazole ring

In complexes **1–3**, every H₂L¹ ligand only joins one metal ion, and in complexes **4** and **5**, every H₂L² ligand links two metal ions; and complex **1** show monomeric structure, complexes **2** and **3** exhibit 1D structures, while **4** and **5** display 3D metal–organic frameworks, as shown in Scheme 2. To the same metal ion and auxiliary ligand, complexes **4** and **5** with H₂L² ligand exhibit higher dimensionality than complexes **2** and **3** with H₂L¹ ligand because the angular between the carboxylate group and the nitrogen coordi-

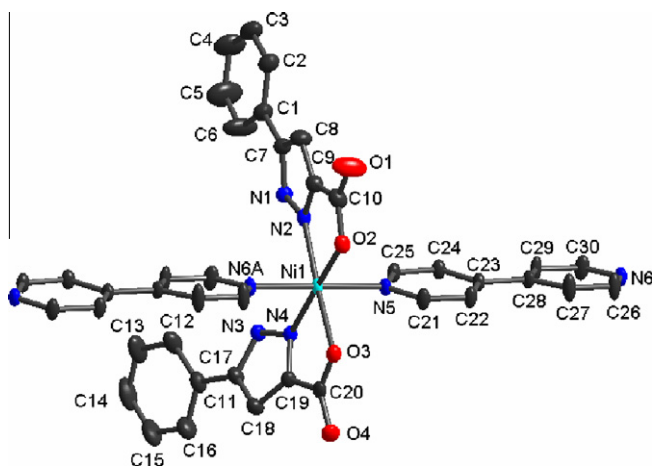


Fig. 3. The coordination environment of Ni(II) ion in complex **2** with 30% thermal ellipsoids. All hydrogen atoms are omitted for clarity (symmetry operation: A: $x + 1/2$, $y + 1/2$, z).

can be viewed as a six-connected node, so the overall structure can be simplified to an unusual (4,6)-connected network with (4⁴·5⁸·6³)(5⁴·6·8) topology, as shown in Fig. 8b. To the best of our knowledge, such a (4,6)-connected network of complex **4** is first reported, which is different from other typical (4,6)-connected net [39–42].

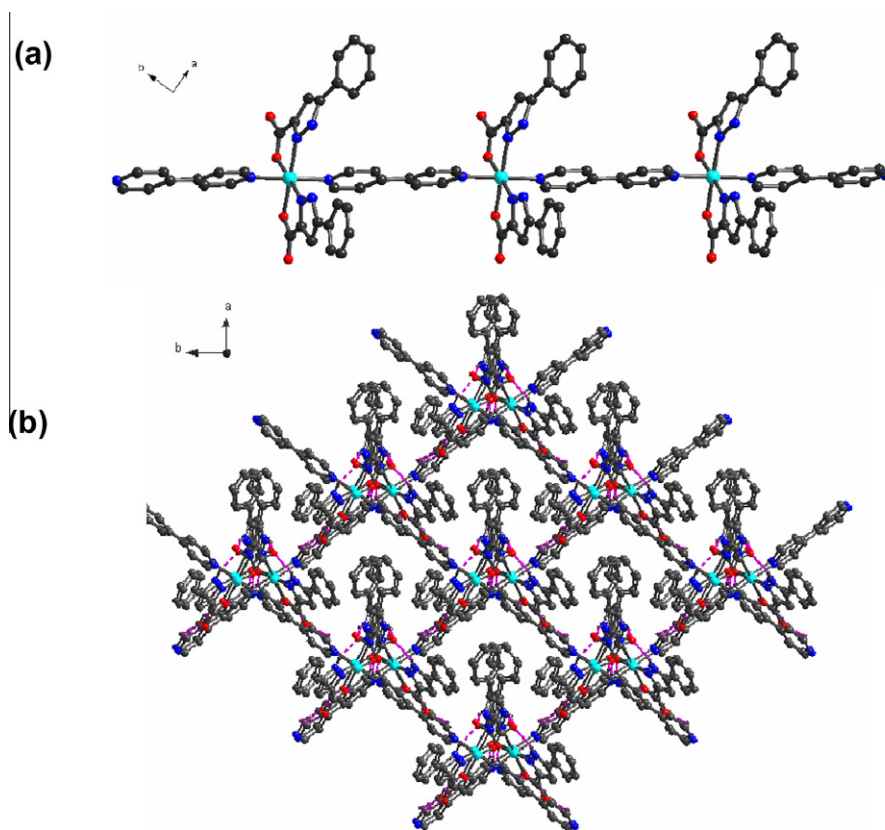


Fig. 4. (a) View of the 1D chain of complex **2** along the *c* axis; (b) The 3D supramolecular network with rhombus channels of **2** along the *c* axis.

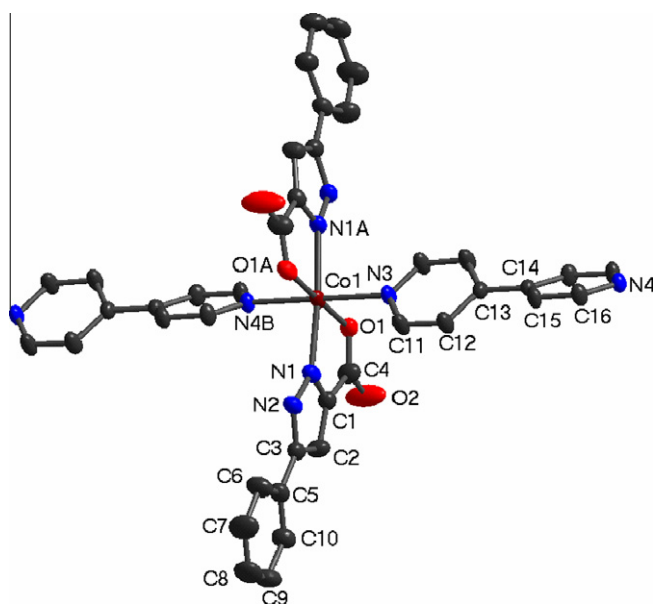


Fig. 5. The coordination environment of Co(II) ion in complex **3** with 30% thermal ellipsoids. All hydrogen atoms are omitted for clarity (symmetry operations: A: $-x + 1, y, -z$; B: $x, y + 1, z$).

nate sites in H_2L^2 is bigger than that in H_2L^1 . In addition, complexes **4** and **5** both contain 1D channels, which show that the angular between O- and N-coordination sites in H_2L^2 help the formation of microporous structures.

3.6.2. Metal ions

With the same ligands H_2L^1 and 4,4'-bipy, Ni complex (**2**) and Co complex (**3**) exhibit different structures. In **2**, both pyrazole nitrogen atoms and carboxylate oxygen atoms are in *cis*-positions, while in **3**, both pyrazole nitrogen atoms and carboxylate oxygen atoms are in *trans*-positions [43]. Moreover, complex **2** exhibits a 3D supramolecular network with rhombus channels, while complex **3** displays a 3D supramolecular network consisting of double-stranded homohelix chains. With the same ligands H_2L^2 and 4,4'-bipy, Ni complex (**4**) and Co complex (**5**) also show different structures. Complex **4** contains binuclear asymmetric units, and exhibits a 3D (4,6)-connected framework with $(4^4 \cdot 5^8 \cdot 6^3)(5^4 \cdot 6 \cdot 8)$ topology, while **5** consists of mononuclear units, and displays a 3D six-connected NaCl-like framework with $(4^{12} \cdot 6^3)$ topology. Furthermore, there are two orientations of H_2L^1 and H_2L^2 ligands in Ni complexes (**2** and **4**), respectively, while only one orientation of H_2L^1 and H_2L^2 ligands in Co complexes (**3** and **5**), respectively. These differences on the structures of complexes **2** and **3** as well as complexes **4** and **5** indicate that a subtle distinction of ionic radius will lead to a completely different structure of complexes for the same ligand and coligand.

3.6.3. Auxiliary ligands

To the same H_2L^1 ligand and Ni(II) ion, complexes **1** and $[Ni(HL^1)_2(H_2O)_2]$ (**6**) reported by our group [30] exhibit monomeric structures, while **2** displays 1D structure. To the same H_2L^2 ligand and Ni(II) ion, complex **4** possesses 3D metal-organic framework, but $[Ni(HL^2)_2(H_2O)_2]$ (**7**) also reported by our group [30] exhibits 1D structure. These results indicate that auxiliary ligand 4,4'-bipy help to enhance the dimensionality of complexes due to its bridging ability, while 2,2'-bipy only joins one metal ion and goes against the formation of high dimensional structures.

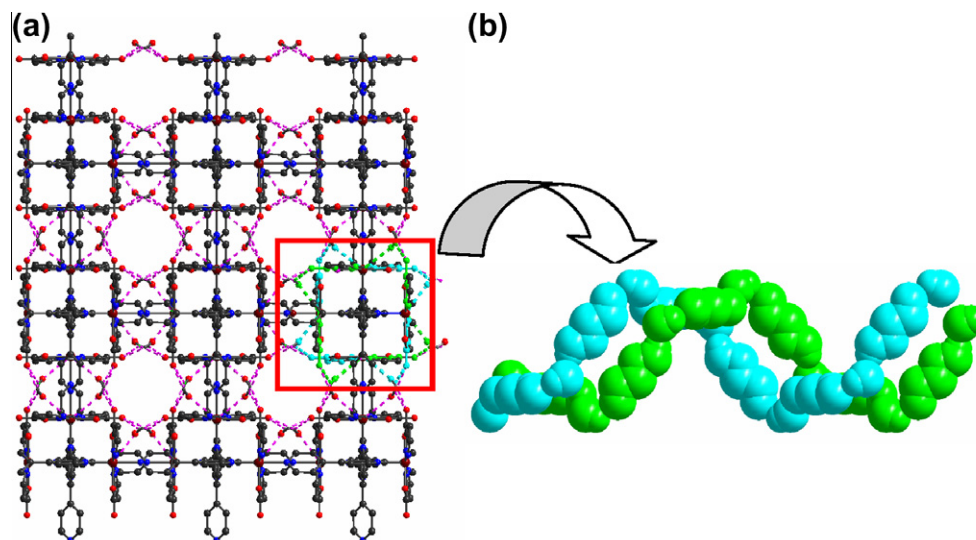


Fig. 6. (a) The 3D supramolecular network consisting of homohelix chains of **3** along the *c* axis, the phenyl rings of HL¹ ligands are omitted for clarity. (b) A left-handed double helical chain consisting of two antiparallel helical chains.

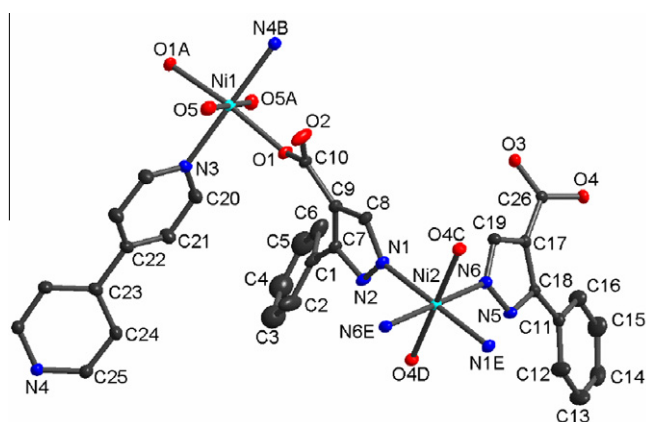


Fig. 7. The coordination environment of Ni(II) ions in complex **4** with 30% thermal ellipsoids. All hydrogen atoms are omitted for clarity (symmetry operations: A: $-x+1/2, y, -z+1$; B: $x, y+1, z$; C: $x+1/2, -y+1, z$; D: $-x, y-1/2, -z+1/2$; E: $-x+1/2, -y+1/2, -z+1/2$).

In addition, of five complexes, only complex **3** crystallize in chiral group, although H₂L¹ and H₂L² ligands are chiral compounds. In general, how to design or make a chiral feature from pairs of enantiomer relies on the understanding of ligands and crystal packing, especially the latter. It remains challenge for the chemists to obtain homochiral crystallization of helical coordination polymers through spontaneous enantiomer selection.

3.7. Thermogravimetric analyses and powder X-ray diffraction

Thermogravimetric (TG) analyses of complexes **1–5** were carried out to examine their thermal stabilities, as shown in Fig. 11. The observed TG curve reveals that complex **1** lost its lattice water molecules at the first weight loss of 8.1% (calcd. 8.4%) from 81 to 124 °C. The TG curve shows a plateau from 124 to 239 °C, then further decomposition began at 239 °C. There are no water molecules in complex **2**, and it was stable up to about 334 °C and then began to decompose with a continuous weight up to above 800 °C. The TG curve of complex **3** reveals a weight loss of 12.9% from 45 to 196 °C, which corresponds to the loss of five lattice water molecules

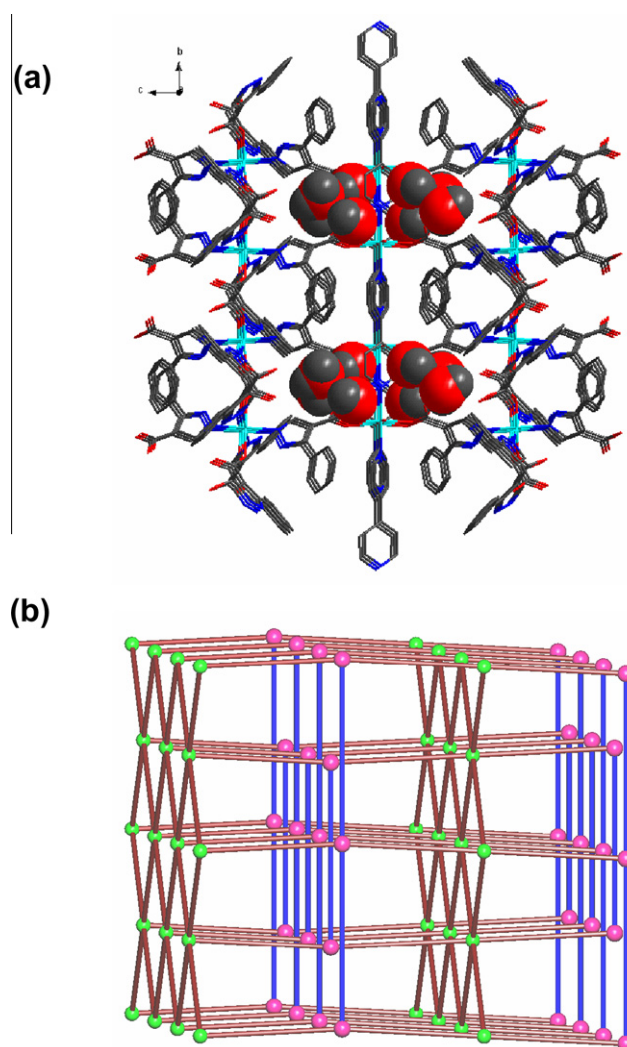


Fig. 8. (a) The 3D metal–organic framework of complex **4** with 1D channels along the *a* axis, the lattice water molecules are shown by spacing-filling model. (b) Schematic representation of a new (4,6)-connected network with (4⁴.5⁸.6³)(5⁴.6.8) topology.

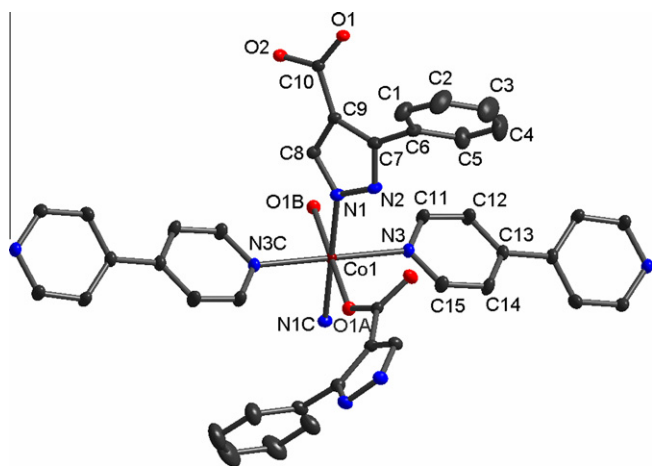
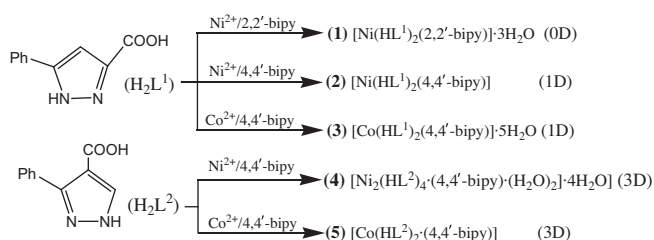


Fig. 9. The coordination environment of Co(II) ion in complex **5** with 30% thermal ellipsoids. All hydrogen atoms are omitted for clarity (symmetry operations: A: $-x + 1/2, y + 1/2, -z + 3/2$; B: $x, -y, z + 1/2$; C: $-x + 1/2, -y + 1/2, -z + 2$).



Scheme 2. Schematic synthesis procedure and the relationship between the dimensionality and the organic ligands of complexes **1–5**.

(calcd. 13.3%). Increasing temperature led to the further decomposition began at 196 °C. For complex **4**, the TG curve displays that the first weight loss of 9.9% from 65 to 133 °C, corresponding to the loss of two coordinated water molecules and four lattice water molecules (calcd. 9.6%). The residue remain stable below 268 °C, and it begins to decompose subsequently above 268 °C. Similar to complex **2**, there are no water molecules in complex **5**, and it was stable up to about 252 °C and then began to decompose with a continuous weight loss up to above 800 °C.

According to the TG analyses, powder XRD patterns of complexes **4** and **5** were recorded. For complex **4**, the powder XRD patterns of the sample at 50 and 150 °C are not the same although very similar, which indicates the change of the frameworks after the removal of lattice and coordinated water molecules. Above 290 °C, the powder XRD patterns change completely, suggesting the collapse of the framework (Fig. 12a). The powder XRD patterns for complex **5** at 100 and 240 °C are the same, indicating that the structural integrity of the framework is maintained. The further decomposition starts at 250 °C, and above 350 °C, the powder XRD patterns change completely, suggesting the collapse of the framework (Fig. 12b).

3.8. Antibacterial activity results

The antibacterial activities of H_2L^1 and H_2L^2 ligands, and complexes **1–5** have been carried out against the selected microorganisms. From the results given in Table 4, it has been observed that all selected compounds show antibacterial activities against Gram positive bacteria: *S. aureus*, *C. albicans* and *B. subtilis*, and Gram

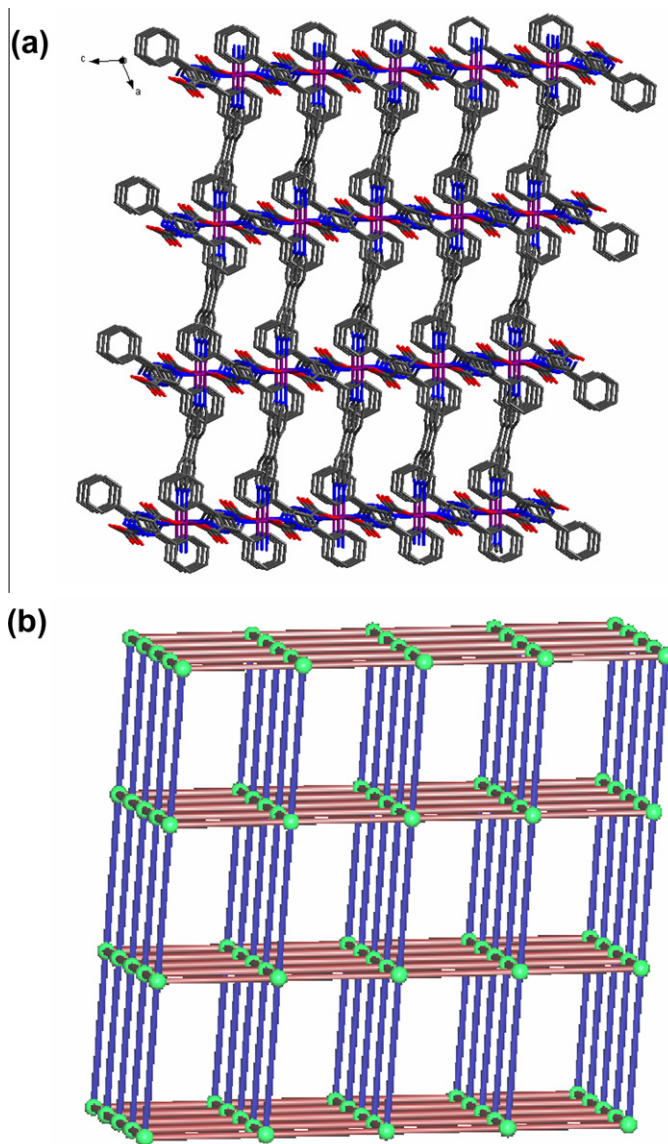


Fig. 10. (a) The 3D metal–organic framework of complex **5** with 1D channels along the b axis. (b) Schematic representation of a six-connected NaCl-like network with $(4^{12}.6^3)$ topology.

negative bacteria: *E. coli* and *P. aeruginosa* at MIC values between 6.25 and 50 $\mu\text{g/mL}$. The complexes have more activities than corresponding free ligands against the tested bacteria. This would imply that the chelation could facilitate the ability of a complex to cross a cell membrane and can be explained by Tweedy's chelation theory [44]. Chelation considerably reduces the polarity of the metal ion because of partial sharing of its positive charge with the donor groups. Such chelation could enhance the lipophilic character of the metal atom, which subsequently favor its permeation through the lipid layers of cell membrane [45].

4. Conclusions

Five new transition metal complexes have been synthesized based on phenyl substituted pyrazole carboxylic acid and N-donor co-ligands. The structural versatilities for the title complexes reveal that different substitution positions of carboxylate group on

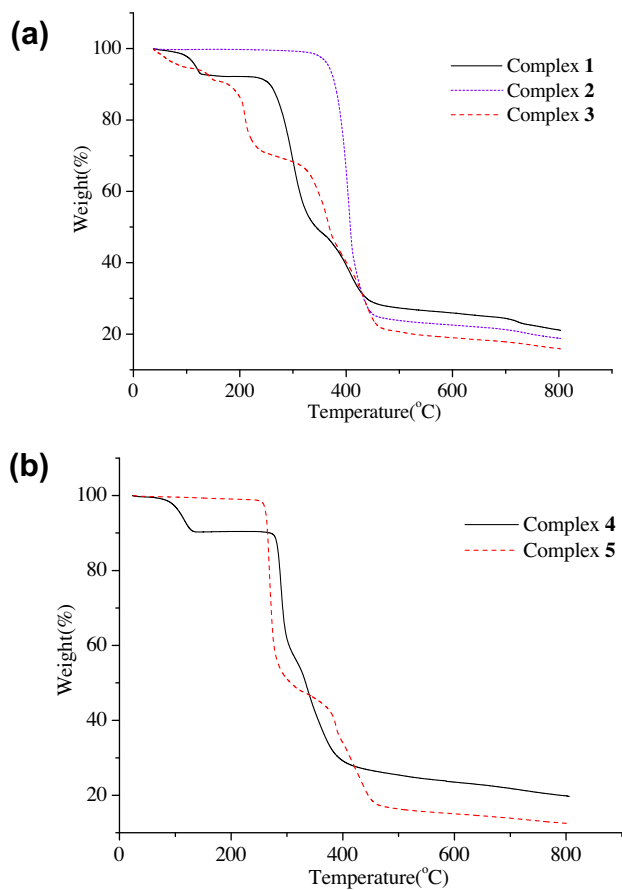


Fig. 11. TG curves of complexes 1–3 (a) and 4 and 5 (b).

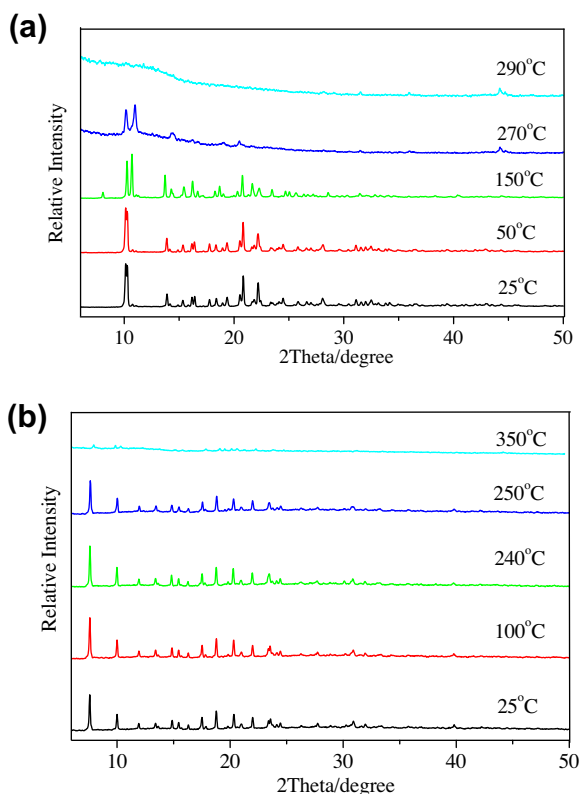


Fig. 12. Powder XRD patterns for complexes 4 (a) and 5 (b) at different temperatures.

Table 4

Minimal inhibitory concentration (MIC) values of H_2L^1 and H_2L^2 ligands, and the title complexes against the tested bacteria ($\mu\text{g/mL}$).

Compound	<i>S. aureus</i>	<i>C. albicans</i>	<i>B. subtilis</i>	<i>E. coli</i>	<i>P. aeruginosa</i>
H_2L^1	25	25	50	50	25
H_2L^2	50	25	25	50	50
1	12.5	12.5	25	25	6.25
2	12.5	6.25	25	12.5	12.5
3	6.25	12.5	6.25	25	12.5
4	12.5	12.5	25	12.5	12.5
5	12.5	12.5	6.25	25	12.5

the pyrazole ring, metal ions and auxiliary ligands have significant effect on the formation and the structures of the resulting complexes. The 3D metal–organic frameworks with 1D channels of complexes **4** and **5** also show that microporous structures can be obtained by changing the angular between O- and N-coordination sites for pyrazole carboxylic acid. In addition, the antibacterial activities screening showed that the complexes have more activity than corresponding free ligand against the tested bacteria.

Acknowledgments

This work was supported by the Natural Science Foundation of China (Grant No. 20961007), the Aviation Fund (Grant No. 2010ZF5 6023) and the Young Scientists Program of Jiangxi Province (Grant No. 2008DQ00600).

Appendix A. Supplementary material

CCDC 824364 (for **1**), 824365 (for **2**), 824366 (for **3**), 824367 (for **4**) and 824368 (for **5**) contain the supplementary crystallographic data for this paper. These data can be obtained free of charge from The Cambridge Crystallographic Data Centre via www.ccdc.cam.ac.uk/data_request/cif. Supplementary data associated with this article can be found, in the online version, at [doi:10.1016/j.ica.2011.11.015](https://doi.org/10.1016/j.ica.2011.11.015).

References

- [1] K. Kavallieratos, J.M. Rosenberg, J.C. Bryan, *Inorg. Chem.* 44 (2005) 2573.
- [2] J.X. Ma, X.F. Huang, X.Q. Song, L.Q. Zhou, W.S. Liu, *Inorg. Chim. Acta* 362 (2009) 3274.
- [3] S. Patil, J. Claffey, A. Deally, M. Hogan, B. Gleeson, L.M.M. Méndez, H. Müller-Bunz, F. Paradisi, M. Tacke, *Eur. J. Inorg. Chem.* (2010) 1020.
- [4] K. Nomiya, K. Onodera, K. Tsukagoshi, K. Shimada, A. Yoshizawa, T. Itoyanagi, A. Sugie, S. Tsuruta, R. Sato, N.C. Kasuga, *Inorg. Chim. Acta* 362 (2009) 43.
- [5] L. Qin, J.S. Hu, L.F. Huang, Y.Z. Li, Z.J. Guo, H.G. Zheng, *Cryst. Growth Des.* 10 (2010) 4176.
- [6] U.O. Ozdemir, P. Guvenc, E. Sahin, F. Hamurcu, *Inorg. Chim. Acta* 362 (2009) 2613.
- [7] Y.F. Han, M. Li, T.W. Wang, Y.Z. Li, Z. Shen, Y. Song, X.Z. You, *Inorg. Chem. Commun.* 11 (2008) 945.
- [8] Z. Su, S.S. Chen, J. Fan, M.S. Chen, Y. Zhao, W.Y. Sun, *Cryst. Growth Des.* 10 (2010) 3675.
- [9] Z. Su, K. Cai, J. Fan, S.S. Chen, M.S. Chen, W.Y. Sun, *CrystEngComm* 12 (2010) 100.
- [10] Q.R. Fang, G.S. Zhu, M. Xue, Z.P. Wang, J.Y. Sun, S.L. Qiu, *Cryst. Growth Des.* 8 (2008) 319.
- [11] W.J. Zhuang, X.J. Zheng, L.C. Li, D.Z. Liao, H. Ma, L.P. Jin, *CrystEngComm* 9 (2007) 653.
- [12] D.C. Zhong, M. Meng, J. Zhu, G.Y. Yang, T.B. Lu, *Chem. Commun.* 46 (2010) 4354.
- [13] J.D. Lin, J.W. Cheng, H.S. Weng, S.W. Du, *Inorg. Chem. Commun.* 11 (2008) 1136.
- [14] F.Q. Wang, W.H. Mu, X.J. Zheng, L.C. Li, D.C. Fang, L.P. Jin, *Inorg. Chem.* 47 (2008) 5225.
- [15] N.C. Kasuga, M. Sato, A. Amano, A. Hara, S. Tsuruta, A. Sugie, K. Nomiya, *Inorg. Chim. Acta* 361 (2008) 1267.
- [16] P. King, R. Clérac, C.E. Anson, A.K. Powell, *Dalton Trans.* (2004) 852.
- [17] C.X. An, Y.C. Lu, Z.F. Shang, Z.H. Zhang, *Inorg. Chim. Acta* 361 (2008) 2721.
- [18] L. Pan, X.Y. Huang, J. Li, Y.G. Wu, N.W. Zheng, *Angew. Chem., Int. Ed.* 39 (2000) 527.

- [19] A.M. Beatty, C.M. Schneider, A.E. Simpson, J.L. Zahera, *CrystEngComm* 4 (2002) 282.
- [20] Z. Shirin, C.J. Carrano, *Polyhedron* 23 (2004) 239.
- [21] M. Frisch, C.L. Cahill, *Dalton Trans.* (2005) 1518.
- [22] P. Roussel, F. Bentiss, M. Drache, P. Conflant, M. Lagrenee, J. Wignacourt, *J. Mol. Struct.* 798 (2006) 134.
- [23] J. Xia, B. Zhao, H.S. Wang, W. Shi, Y. Ma, H.B. Song, P. Cheng, D.Z. Liao, S.P. Yan, *Inorg. Chem.* 46 (2007) 3450.
- [24] J. Zhao, L.S. Long, R.B. Huang, L.S. Zheng, *Dalton Trans.* (2008) 4714.
- [25] Q. Shi, Y.T. Sun, L.Z. Sheng, K.F. Ma, X.Q. Cai, D.S. Liu, *Inorg. Chim. Acta* 362 (2009) 4167.
- [26] M. Maekawa, T. Tominaga, T. Okubo, T. Kuroda-Sowa, M. Munakata, *Eur. J. Inorg. Chem.* (2009) 4225.
- [27] J. Shen, C.C. You, S. Wu, *Chin. J. Pharm.* 31 (2000) 419.
- [28] F. Wei, B.X. Zhao, B. Huang, L. Zhang, C.H. Sun, W.L. Dong, D.S. Shin, J.Y. Miao, *Bioorg. Med. Chem. Lett.* 16 (2006) 6342.
- [29] A.V. Lebedev, A.B. Lebedeva, *Russ. J. Gen. Chem.* 75 (2005) 782.
- [30] Y.N. Gong, C.B. Liu, H.L. Wen, L.S. Yan, Z.Q. Xiong, L. Ding, *New J. Chem.* 35 (2011) 865.
- [31] Q. Chu, G.X. Liu, Y.Q. Huang, X.F. Wang, W.Y. Sun, *Dalton Trans.* (2007) 4302.
- [32] J.P. Zhang, S. Kitagawa, *J. Am. Chem. Soc.* 130 (2008) 907.
- [33] P. Kanoo, T.K. Maji, *Eur. J. Inorg. Chem.* (2010) 3762.
- [34] M.H. Zeng, S. Hu, Q. Chen, G. Xie, Q. Shuai, S.L. Gao, L.Y. Tang, *Inorg. Chem.* 48 (2009) 7070.
- [35] F. Costantino, A. Ienco, S. Midollini, A. Orlandini, A. Rossin, L. Sorace, *Eur. J. Inorg. Chem.* (2010) 3179.
- [36] G.M. Sheldrick, *SADABS*, Program for Empirical Absorption Correction of the Area Detector Data, University of Göttingen, Germany, 1997.
- [37] G.M. Sheldrick, *SHELXS-97*, Program for Crystal Structure Solution, University of Göttingen, Germany, 1997.
- [38] G.M. Sheldrick, *SHELXL-97*, Program for Crystal Structure Refinement, University of Göttingen, Germany, 1997.
- [39] Y.Q. Lan, S.L. Li, X.L. Wang, K.Z. Shao, D.Y. Du, H.Y. Zang, Z.M. Su, *Inorg. Chem.* 47 (2008) 8179.
- [40] S.L. Li, Y.Q. Lan, J.F. Ma, J. Yang, G.H. Wei, L.P. Zhang, Z.M. Su, *Cryst. Growth Des.* 8 (2008) 675.
- [41] Z.H. Weng, Z.L. Chen, F.P. Liang, *Inorg. Chem.* 48 (2009) 8703.
- [42] Y. Zhang, T. Wu, R. Liu, T. Dou, X.H. Bu, P.Y. Feng, *Cryst. Growth Des.* 10 (2010) 2047.
- [43] A. Das, S.M. Peng, S. Bhattachary, *Polyhedron* 19 (2000) 1227.
- [44] B.G. Tweedy, *Phytopathology* 55 (1964) 910.
- [45] M. Tumer, D. Ekinci, F. Tumer, A. Bulut, *Spectrochim. Acta, Part A: Mol. Biomol. Spectrosc.* 67 (2007) 916.